JOURNAL OF MOLECULAR SPECTROSCOPY **147**, 27–39 (1991)

The Submillimeter Rotation Tunneling Spectrum of the Water Dimer

E. ZWART, J. J. TER MEULEN, AND W. LEO MEERTS

Fysisch Laboratorium, University of Nijmegen, Toernooiveld, 6525 ED Nijmegen, The Netherlands

AND

L. H. COUDERT

Laboratoire de Physique Moléculaire et Atmosphérique, Université Pierre et Marie Curie et CNRS, Tour 13-4 Place Jussieu, 75252 Paris Cedex 05, France

Rotational tunneling transitions have been measured for the ($K_a = 0$, lower) → ($K_a = 1$, upper) and the ($K_a = 1$, lower) → ($K_a = 2$, upper) bands of $(H_2O)_2$. Although some of these transitions have been reported in an earlier publication, a more detailed discussion of the experiment and of the results is presented here. Transitions have been measured by direct absorption spectroscopy in a continuous slit nozzle expansion using either harmonics from klystrons or sidebands. These data along with previous measurements have been analyzed using an IAM-like treatment. A better determination of the A rotational constant and of the value of the largest tunneling splitting has been achieved.

1 INTRODUCTION

The water dimer has been the subject of much spectroscopic work during the past years. The initial goal of this research was to gain a better understanding of the interaction between the two monomers. If this interaction were fully understood, the interaction between three or more monomers could be investigated, leading to a better understanding of the condensation process. However, the structure and dynamics of the dimer have turned out to be difficult and, most of all, interesting enough to direct most of the work done until now at the dimer form.

The first MBER measurements of Dyke *et al.* (*1*) established the structure of the water dimer to be like the one drawn in Fig. 1. There is a single hydrogen bond between the two monomers. Later microwave (*2–7*), far infrared (*8*), and infrared (*9, 10*) measurements and theoretical works (*11–13*) elucidated many details of the ground vibrational state in which several tunneling splittings arise because of large amplitude motions. All measurements were included in a fit, recently published by Coudert and Hougen (*14*).

In spite of the vast amount of spectroscopic effort, there is still uncertainty about the exact magnitude of the A rotational constant and about the value of the largest tunneling splitting, caused by the motion in which the hydrogen acceptor monomer rotates over 180°, interchanging its two hydrogen atoms. In the analysis of Coudert and Hougen (*14*) an accurate determination of these two parameters could not be carried out because they were correlated. Information on the nondegenerate tunneling

0022-2852/91 $3.00

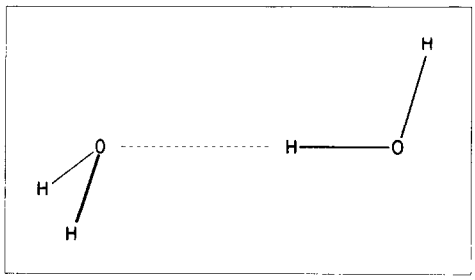

FIG. 1. The equilibrium structure of $(H_2O)_2$.

states in ($K_a = 1$, upper) was also missing and the magnitude of the tunneling splitting caused by the two interconversion large amplitude motions was not known for these states.

In a recent letter (*15*) we have reported the observation of several submillimeter $\Delta K_a = 1$ transitions. In the present paper the experiment and the results are discussed in more detail. Further, a new band and supplementary measurements are presented. All data are analyzed using the same formalism as that utilized by Coudert and Hougen (*14*), resulting in a better determination of the A rotational constant and of the magnitude of the largest tunneling splitting. More insight is also gained on the rotational dependence of the tunnel splittings.

2 EXPERIMENTAL DETAILS

The spectrometer used in this work has been described in detail elsewhere (*16*). Here its basic operation will be briefly explained. Its use for harmonic generation is discussed somewhat more in detail, since this is essential for this paper and is not included in Ref. (*16*).

The radiation is generated with a tunable sideband spectrometer (see Fig. 2). The FIR laser is a molecular laser pumped by a 150-W CO_2 laser. By using different gases

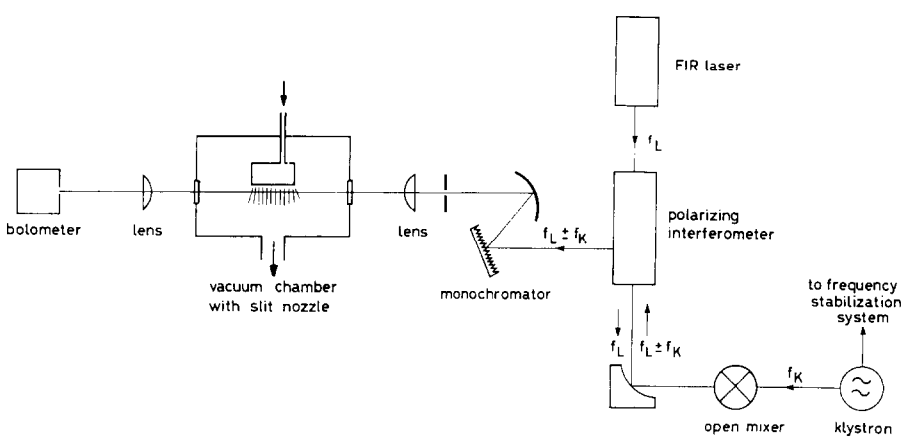

FIG. 2. The FIR spectrometer.

(e.g., CH_3OH, HCOOC) in the molecular laser and different pump lines from the CO_2 laser, approximately 30 strong (50 mW) FIR laser frequencies can be reached. By mixing the fixed frequency FIR laser radiation with tunable microwave radiation, tunable sum and difference frequencies (sidebands) are generated. The tunable microwave radiation is generated by klystrons (100 mW) in the 55–114 GHz range.

The generation of the sidebands takes place in an open structure mixer with a GaAs Schottky barrier diode. The microwave radiation is coupled onto the diode by a pin in the waveguide and the FIR radiation by an antenna. The sidebands are radiated by the antenna into free space. The antenna pattern is improved by a corner reflector.

The tunable sidebands are separated from the much stronger laser radiation by a polarizing interferometer and a monochromator. The monochromator transmits either the sum or the difference frequency and this radiation is passed through the vacuum chamber where the absorption takes place. A Si bolometer at 1.5 K is used for the detection of the absorption signals.

This spectrometer can also be used for harmonic generation in the region 300–450 GHz by removing the FIR laser radiation. The harmonics are radiated into free space by the antenna of the mixer and are directed, like the sidebands, through the optical elements to the detector by mirrors and lenses. The antenna length used in both cases (sidebands and harmonics) is approximately 2 mm.

Previously we had to replace the grating (30° blaze angle, 3 grooves/mm) of the monochromator by a mirror, because this grating did not operate below 550 GHz. The different harmonics were then separated by a Fabry Perot (10 lines/mm mesh). More recently a new grating (30° blaze angle, 1.33 grooves/mm) allows us to use the monochromator down to 300 GHz, which simplifies the operation of the spectrometer.

With the calibrated monochromator it is easy to select the harmonic needed for the experiment. The harmonic is optimized in the same way as the sidebands are. Coupling of the microwave power onto the diode is optimized with a movable plunger at the end of the waveguide. The corner reflector, which determines the antenna pattern, is set for highest power. Changing the bias voltage on the diode, the radiated power varies from zero to a maximum, with usually more than one maximum for the range of bias voltages used. The optimum bias voltage is different for every harmonic and depends on the incident microwave power.

The power of the generated harmonics is more than linearly dependent on the microwave power. With the available klystrons (approximately 100 mW), we cannot saturate the diode. Because of this only the most powerful klystrons are used. In our case this means using the 5th and 6th harmonic of klystrons around 60 GHz or the 4th and 5th harmonic of klystrons around 100 GHz.

The powers which can be generated for harmonics and sidebands are of the same order of magnitude. The frequency of the harmonics is precisely known, because the klystrons are phase locked to a frequency standard. The frequency uncertainty of the sidebands is determined by the FIR laser. The uncertainty in the frequency of transitions measured with harmonics we estimate to be 0.1 MHz and of those with sidebands 1.0 MHz. The minimum fractional absorption obtainable with this spectrometer is approximately 10^{-5}.

The absorption takes place in a vacuum chamber with a continuously operating slit nozzle, pumped by a 4000 m^3/h roots pump. The 4000 m^3/h roots pump is

backed by a 1200 m^3/h roots pump and a 80 m^3/h rotary pump. The slit is 4 cm long and 25–50 μm wide. Its design is similar to the one described by Busarow *et al.* (*17*). We used a backing pressure of 500 Torr Ar with a few percent H_2O. The pressure in the vacuum chamber was 0.1 mbar. The beam of radiation is focused to a diameter of 5 mm as it passes 10 mm from the nozzle.

Due to the slit nozzle expansion, the linewidths are approximately three times smaller than linewidths obtained in an absorption cell or a pinhole expansion. Typical linewidths are 500 kHz full width at half-maximum. We use frequency modulation with $2f$ ($2f$ = 1 kHz) lock in detection. Because of the limited speed of the bolometer we cannot use a higher modulation frequency.

In the expansion of H_2O and Ar, several complexes $(Ar)_n(H_2O)_m$ are formed. To check whether the transitions are not due to a complex with Ar, we substituted Ar with Kr. For $(H_2O)_2$ transitions the intensity dropped to approximately one-third of the value obtained with Ar.

3 RESULTS

Many details of the energy level diagram of the water dimer have been determined by previous microwave, far infrared, and infrared measurements (see Fig. 3 and Introduction for references). The water dimer is a near symmetric rotor in which four large amplitude motions lead to a splitting of the rotational levels into six sublevels. As stated by Dyke (*11*), the molecular symmetry group to be used is G_{16} and the six sublevels belong to one of the following symmetry species of this group: $A_1^{\pm}$, $E^{\mp}$, $B_1^{\pm}$, $A_2^{\mp}$, $E^{\mp}$, $B_2^{\mp}$, where the upper (lower) sign is convenient when the symmetry species of the rotational level in the point group C_s of the dimer equilibrium configuration is A' (A''). For the understanding of the measured bands, the four large amplitude motions as well as their effect will be briefly described below.

The most feasible tunneling motion corresponds to a 180° rotation of the acceptor monomer, resulting in an exchange of the two hydrogen atoms of this monomer. As can be seen in Fig. 3, this motion separates the six tunneling sublevels into two sets: the first set corresponds to the three levels belonging to the symmetry species $A_1^{\pm}$, $E^{\pm}$, and $B_1^{\pm}$; the second set to the three levels belonging to the symmetry species $A_2^{\mp}$, $E^{\mp}$, and $B_2^{\mp}$. From here on, for a given K_a value and depending on the relative energy of the two sets, one of them will be referred to as (K_a, upper) and the other one as (K_a, lower). The tunneling splitting associated with this large amplitude motion varies with K_a; for $K_a = 0$ it is about 280 GHz. One of the results of the present work is a good determination of this number (see Table II).

The water dimer displays two different interconversion motions. The more feasible one involves geared rotations of the two monomer units while the other and less feasible one involves antigeared rotations of the same units. As emphasized by Fig. 3, these two tunneling motions shift the A_1^-, A_2^+, B_1^+, and B_2^- levels up and the A_1^+, A_2^-, B_1^-, and B_2^+, levels down; the positions of the doubly degenerate levels are unaffected. The magnitude of the splitting is exaggerated in the figure. Depending on the set of levels being considered, the effects of the two interconversion motions are constructive or destructive. For $K_a = 0$, the interconversion tunneling splitting is about 22.5 GHz for the lower set and 19.5 GHz for the upper set.

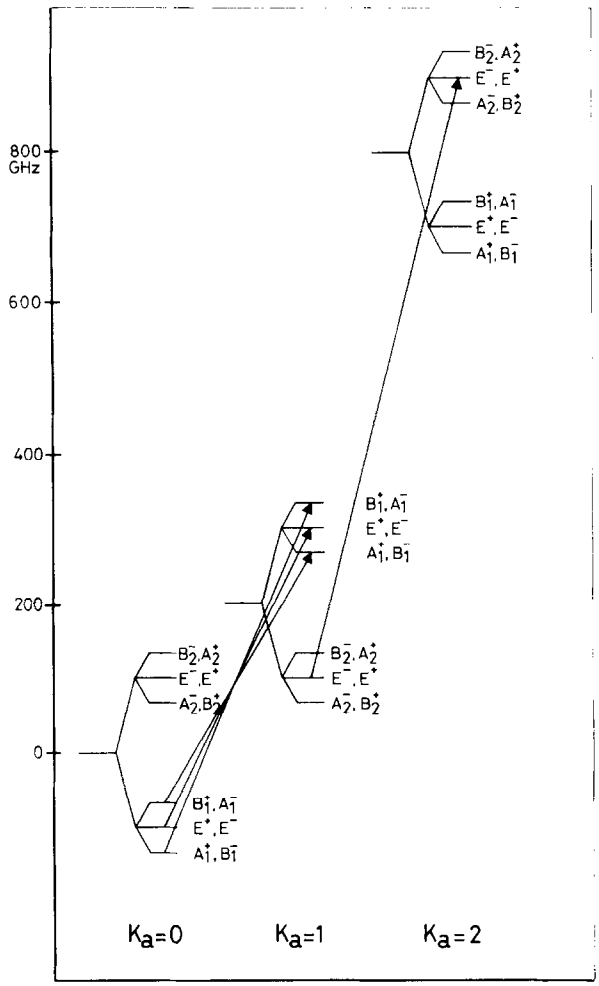

FIG. 3. The energy level scheme of the ground vibrational state of $(H_2O)_2$.

The fourth tunneling motion displayed by the water dimer is, from the point of view of feasibility, somewhere in between the two interconversion motions just described. This motion leads to an exchange of the donor monomer hydrogen atoms but does not further split the tunneling sublevels. It merely shifts the levels up or down depending on whether they are nondegenerate or doubly degenerate. The effects of this last tunneling motion are not taken into account in Fig. 3.

As in Ref. (*14*), the four tunneling motions are conveniently labeled using the number of the framework reached when starting the motion from framework number 1 (*13*). Thus, using the framework numbering of Ref. (*12*), the four previous tunneling motions in order of decreasing feasibility are the $1 \rightarrow 4$, $1 \rightarrow 5$, $1 \rightarrow 2$, and $1 \rightarrow 7$, the second and last labels being for the geared and antigeared interconversion motion, respectively. This labeling is also useful to characterize the parameters of each tunneling motion.

To understand the spectrum we observed, we must keep in mind that the selection rules are: $\Delta J = 0, \pm 1$; $\Delta K_a = 0, 1$; $A_1^+ \leftrightarrow A_1^-$, $B_1^+, \leftrightarrow B_1^-$, $A_2^+, \leftrightarrow A_2^-$, $B_2^+ \leftrightarrow B_2^-$, $E^+ \leftrightarrow E^-$. The possible transitions for ($K_a = 0$, lower) → ($K_a = 1$, upper) are drawn in Fig. 3. Since the rotational energy for a near prolate asymmetric rotor (with a given K_a) has to be superimposed on the drawn levels, the transitions will form three bands, similar to vibrational bands, with a P, Q, and R branch. As is clear from Fig. 3, the bands can be denoted by the symmetries of the initial levels. (For example, band (A_1^+, B_1^-) with transition $P(4)A_1^+$). In the same way, for $K_a = 1 \rightarrow K_a = 2$ there will be six bands, three originating from ($K_a = 1$, lower) and three from ($K_a = 1$, upper). The band originating in ($K_a = 1$, lower), which is presented in this paper, has also been drawn in Fig. 3.

3.1 ($K_a = 0$, lower) → ($K_a = 1$, upper)

From the above it is clear that the band origin of ($K_a = 0$, lower) → ($K_a = 1$, upper) could not be determined very accurately from previous measurements. This origin lies at $A + \Delta\nu$, where A is the rotational constant and $\Delta\nu$ contains the effects of the largest tunneling splitting (the effects of the other tunneling motions are ignored for simplicity). At the time of the measurements only $A - \Delta\nu$ was known precisely (*6, 7*) and, although A and $\Delta\nu$ could have been calculated separately from Ref. (*14*), the values obtained would not have been very reliable due to the fact that these two parameters were correlated in the analysis presented there.

However, the relative positions of several transitions in the band were known, because of combination differences with microwave transitions in $K_a = 0$ and $K_a = 1$. Further, the band extends over a large frequency region. Therefore, once one transition had been found, the rest of the band followed by guessing the assignment of the obtained transition.

In Ref. (*15*) the frequencies of the transitions we measured with harmonic generation can be found. These consist of three bands, with initial levels respectively (A_1^+, B_1^-), (B_1^+, A_1^-), and (E^+, E^-). Since $B_1^\pm$ levels have 0 statistical weight, one transition out of two is missing in the first and second band. With the sideband system we have measured some additional transitions at higher frequencies. The R-branch measurements were extended to higher J to get some more data for the fit, which did not work very well for the limited set of $A_1^\pm$ transitions reported in Ref. (*15*). In the original measurements with harmonic generation there were some problems with the assignment of the Q branch involving levels of (A_1^+, B_1^-) symmetry. With the sideband system, more power could be generated at the corresponding wavelength and a definite assignment could be made (see Fig. 4). The transition originally assigned as $Q(2)$ split up into two, now assigned as $Q(2)$ and $Q(4)$. This means that the transition originally called $Q(4)$ is actually $Q(6)$; also $Q(8)$ was found. The relative intensities of the $Q(2)$–$Q(8)$ transitions are consistent with those found for other $(H_2O)_2$ Q branches. $A_1^\pm$ levels have a statistical weight which is three times smaller than that of $E^\pm$ levels. In our spectra, the transitions between $E^\pm$ levels had a signal-to-noise ratio of 50 and the transitions between $A_1^\pm$ levels 10 (with an RC time of 3 s). An effect which was also seen by Busarow *et al.* (*8*) is that P-branch transitions are approximately three times weaker than Q- and R-branch transitions. The complete list of measured

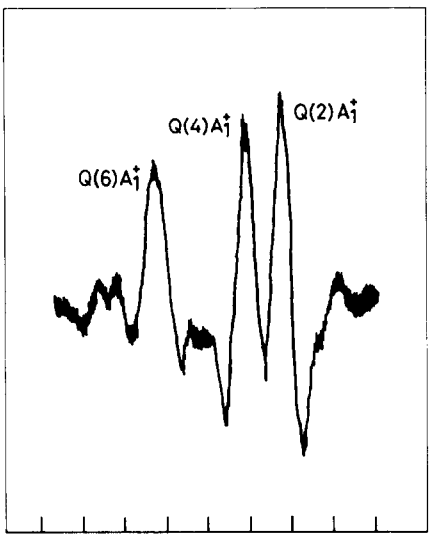

FIG. 4. Three-Q-branch transitions. The distance between frequency markers is 1 MHz.

transitions can be found in Table I. The notation used in this table is the same as in Ref. (*14*).

For the $E^{\pm}$ symmetry levels, microwave measurements were available for both $K_a = 0$ and $K_a = 1$ and the assignment of many transitions from the P, Q, and R branches could be checked using combination differences. However, it turned out that the transitions within ($K_a = 1$, upper) were misassigned in Refs. (*4, 6*); the levels were not assigned the proper component of the K-type doubling. A relabeling was carried out changing the K-type doubling component and making the change $E^{\pm} \rightarrow E^{\mp}$ in the symmetry species labels. Unexpectedly, the K-type doubling "changes" for the doubly degenerate levels in ($K_a = 1$, upper); more precisely, the levels for which the contribution from the asymmetry is $+ 1/4\,(B - C)J(J + 1)$ are below those for which this contribution is $- 1/4(B - C)J(J + 1)$. For the $A_1^{\pm}$ levels, microwave measurements were only available for $K_a = 0$. Therefore only P and R transitions with a common final level could be checked.

3.2 ($K_a = 1$, lower) → ($K_a = 2$, upper)

The (A_2^-, B_2^+), and (B_2^-, A_2^+), bands of ($K_a = 1$, lower) → ($K_a = 2$, upper) were published by Busarow *et al.* (*8*). The assignment in terms of upper or lower is not yet certain for $K_a = 2$. These bands were relatively strong, as strong as those described in the previous section, since they originate from levels which cannot relax to lower levels and which are, therefore, well populated (*3*). However, the $E^{\pm}$ ($K_a = 1$, lower) levels can relax to the $E^{\pm}$ ($K_a = 0$, lower) levels and we expect the former levels to be much less populated than the latter ones. The energy difference between the two sets of levels being about 200 GHz, the $E^{\pm}$ ($K_a = 1$, lower) levels are seven times less populated than the $E^{\pm}$ ($K_a = 0$, lower) levels in a 5-K jet. It is worthwhile pointing out that this ratio depends very strongly on the temperature in the jet.

TABLE I

Assignment, Measured Frequencies, and Observed Minus Calculated Differences in the Spectrum of the Water Dimer

J'	±K'[a]	Γ'[b]	J"	±K"[a]	Γ"[b]	FREQ[c]	REF[c]	O-C[d]	J'	±K'[a]	Γ'[b]	J"	±K"[a]	Γ"[b]	FREQ[c]	REF[c]	O-C[d]
1	0	E-	0	0	E+	12320.997	[1,3]	0.10	2	-1	B2-	2	1	B2+	16918.527	[3]	-0.05
2	0	E+	1	0	E-	24640.807	[1,3]	0.17	2	1	A2+	2	-1	A2-	15544.205	[3]	-0.01
3	0	E-	2	0	E+	36958.13	[6]	0.08	3	-1	B2+	2	-1	B2-	21189.816	[3]	0.03
4	0	E+	3	0	E-	49271.94	[6]	-0.03	3	1	A2-	2	1	A2+	20620.650	[3]	-0.10
5	0	E-	4	0	E+	61580.86	[6]	-0.37	3	-1	A2+	2	-1	A2-	53753.29	[6]	-0.08
6	0	E+	5	0	E-	73884.03	[6]	-0.64	3	1	B2-	2	1	B2+	53015.86	[6]	-0.03
7	0	E-	6	0	E+	86179.50	[6]	-1.61	3	1	B2-	3	-1	B2+	14907.528	[3]	0.00
1	0	E+	0	0	E-	12132.810	[2,4,5]	-0.08	3	-1	A2+	3	1	A2-	17588.410	[3]	0.00
2	0	E-	1	0	E+	24284.320	[4,5]	-0.25	4	1	A2+	3	1	A2-	65275.95	[6]	-0.01
3	0	E+	2	0	E-	36464.94	[6]	-0.52	4	-1	B2-	3	-1	B2+	66233.20	[6]	-0.10
4	0	E-	3	0	E+	48675.12	[6]	-0.98	4	1	B2+	3	1	B2-	32895.28	[6]	-0.16
1	0	A2+	0	0	A2-	31673.40	[7]	0.25	4	-1	A2-	3	-1	A2+	33594.83	[6]	0.08
1	0	B2+	0	0	B2-	-7354.864	[2,3]	0.00	4	-1	B2-	4	1	B2+	18430.396	[4]	0.06
2	0	A2-	1	0	A2+	4863.160	[2]	0.05	4	1	A2+	4	-1	A2-	14092.803	[4]	0.00
2	0	B2-	1	0	B2+	43797.03	[6]	0.54	5	1	A2-	4	1	A2+	45167.86	[6]	0.27
3	0	B2+	2	0	B2-	17122.618	[2,3]	0.03	5	-1	B2+	4	-1	B2-	45978.83	[6]	0.05
3	0	A2+	2	0	A2-	55916.67	[6]	0.57	5	-1	A2+	4	-1	A2-	78678.88	[6]	0.39
4	0	B2-	3	0	B2+	68043.50	[6]	0.57	5	1	B2-	5	-1	B2+	13120.210	[4]	-0.03
4	0	A2-	3	0	A2+	29416.387	[2]	-0.01	5	-1	A2+	5	1	A2-	19418.12	[6]	0.02
5	0	B2+	4	0	B2-	41734.73	[6]	-0.08	6	1	A2+	5	1	A2-	89775.12	[6]	0.19
5	0	A2+	4	0	A2-	80182.68	[6]	0.47	6	-1	B2-	5	-1	B2+	91086.90	[6]	0.66
6	0	A2-	5	0	A2+	54068.53	[6]	-0.13	6	1	B2+	5	1	B2-	57436.73	[6]	0.74
6	0	B2-	5	0	B2+	92334.56	[6]	-0.17	6	1	A2+	6	-1	A2-	12008.176	[4]	-0.04
7	0	B2+	6	0	B2-	66410.42	[6]	-0.21	7	1	B2-	7	-1	B2+	10772.506	[4]	0.02
8	0	A2-	7	0	A2+	78755.59	[6]	0.22	5	-1	A2+	6	0	A2-	-36804.25	[7]	-0.18
9	0	B2+	8	0	B2-	91099.28	[6]	0.25	4	-1	B2-	5	0	B2+	-25899.06	[6]	-0.38
1	0	A1-	0	0	A1+	34871.38	[7]	0.13	3	-1	A2+	4	0	A2-	-14826.98	[6]	-0.54
2	0	A1+	1	0	A1-	2110.358	[4]	0.02	1	1	B2-	1	0	B2+	32112.47	[7]	0.66
3	0	A1-	2	0	A1+	59465.85	[6]	0.04	2	1	A2+	2	0	A2-	32297.22	[6]	0.33
4	0	A1+	3	0	A1-	26810.57	[6]	-0.05	3	1	B2-	3	0	B2+	32553.28	[6]	0.00
5	0	A1-	4	0	A1+	84001.67	[6]	-0.04	4	1	A2+	4	0	A2-	32860.80	[6]	-0.31
6	0	A1+	5	0	A1-	51535.65	[6]	-0.50	5	1	B2-	5	0	B2+	33199.97	[7]	-0.37
7	0	A1-	6	0	A1+	108469.87	[6]	-0.10	6	1	A2+	6	0	A2-	33552.54	[7]	-0.23
1	-1	E+	1	1	E-	259.915	[4]	0.00	7	1	B2-	7	0	B2+	33903.33	[7]	0.45
2	-1	E-	2	1	E+	759.741	[4]	-0.05	2	-1	A2-	1	0	A2+	21616.23	[6]	0.45
3	-1	E+	3	1	E-	1468.081	[4]	-0.05	3	-1	B2+	2	0	B2-	34768.42	[6]	0.08
4	-1	E-	4	1	E+	2351.680	[4]	-0.05	1	0	E+	2	-1	E-	-36609.62	[7]	0.85
5	-1	E+	5	1	E-	3381.641	[4]	-0.05	3	0	E+	2	-1	E-	24139.64	[7]	0.07
1	1	E+	1	-1	E-	5.096	[4]	0.03	4	0	E-	3	-1	E+	35286.60	[7]	-0.94
2	1	E-	2	-1	E+	15.301	[4]	0.08	3	-1	A1-	4	0	A1+	404054.90	[15]	-1.52
3	1	E+	3	-1	E-	30.543	[4]	0.05	2	-1	A1+	3	0	A1-	372784.99	[15]	-0.45
4	1	E-	4	-1	E+	50.819	[4]	-0.13	1	-1	A1-	2	0	A1+	428731.67	[15]	0.30
2	1	E+	1	1	E-	24548.297	[4]	-0.20	1	1	A1+	1	0	A1-	409708.10	[15]	-0.17
2	-1	E-	1	-1	E+	25048.436	[4]	0.06	2	1	A1-	2	0	A1+	453392.0	WRK	0.66
2	1	E+	1	-1	E+	24288.537	[4]	-0.04	3	1	A1+	3	0	A1-	409815.62	[15]	0.56
3	-1	E+	2	-1	E-	37528.24	[6]	0.11	4	1	A1-	4	0	A1+	453392.8	WRK	1.11
3	1	E-	2	1	E+	36819.84	[6]	0.05	5	1	A1+	5	0	A1-	410008.91	[15]	1.14
4	1	E+	3	1	E-	49087.66	[6]	0.10	6	1	A1-	6	0	A1+	453395.29	[15]	0.98
4	-1	E-	3	-1	E+	49971.38	[6]	0.22	7	1	A1+	7	0	A1-	410287.20	[15]	0.01
2	-1	E+	1	-1	E-	24654.344	[4]	-0.01	8	1	A1-	8	0	A1+	453400.3	WRK	-1.62
2	1	E-	1	1	E+	24664.549	[4]	0.05	1	-1	A1-	0	0	A1+	465713.34	[15]	0.38
2	1	E-	1	-1	E-	24669.651	[4]	0.08	2	-1	A1+	1	0	A1-	434361.24	[15]	-0.35
3	1	E+	2	1	E-	36993.72	[6]	-0.12	3	-1	A1-	2	0	A1+	490332.0	WRK	0.86
3	-1	E-	2	-1	E+	36978.50	[6]	-0.06	4	-1	A1+	3	0	A1-	459083.49	[15]	-0.71
4	-1	E+	3	-1	E-	49299.16	[6]	-0.05	5	-1	A1-	4	0	A1+	514910.9	WRK	-3.93
4	1	E-	3	1	E+	49319.49	[6]	-0.18	6	-1	A1+	5	0	A1-	483844.2	WRK	-1.16
1	1	B2-	1	-1	B2+	15982.874	[3]	-0.03	7	-1	A1-	6	0	A1+	539441.2	WRK	-9.48
1	-1	A2+	1	1	A2-	16449.424	[3]	-0.05	8	-1	A1+	7	0	A1-	508633.2	WRK	-2.47
2	1	B2+	1	1	B2-	8344.588	[3]	-0.07	4	-1	E+	5	0	E-	367308.53	[15]	0.06
2	-1	A2-	1	-1	A2+	8756.579	[3]	-0.01	3	-1	E-	4	0	E+	379590.38	[15]	-0.11

[a] These columns give the K assignment of the levels. The -K and +K notation is explained in Ref. [14].

[b] Γ is the symmetry species of the level in the group G_{16}.

[c] FREQ is the measured frequency in MHz, as taken from the reference(s) in the REF column or from this work when WRK is written.

[d] O-C is the observed minus calculated difference calculated with the constants in Table II.

For the $E^{\pm}$ levels, microwave measurements were available for both $K_a = 1$ and $K_a = 2$. This gave us the relative positions of the low J transitions of the band. An estimate of the band origin could have been carried out using the results of Ref. (*8*) and assuming that it lies between the two bands measured in this reference. However, this estimation was not deemed accurate enough since it involves neglecting the effects of the $1 \rightarrow 2$

TABLE I—*Continued*

J'	±K'[a]	Γ'[b]	J"	±K"[a]	Γ"[b]	FREQ[c]	REF[c]	O-C[d]	J'	±K'[a]	Γ'[b]	J"	±K"[a]	Γ"[b]	FREQ[c]	REF[c]	O-C[d]
2	-1	E+	3	0	E-	391883.86	[15]	-0.04	4	2	B2-	3	-1	B2+	719463.0	[8]	1.25
1	-1	E-	2	0	E+	404187.79	[15]	0.20	5	-2	A2-	4	1	A2+	705953.9	[8]	-0.21
1	1	E+	1	0	E-	428833.58	[15]	0.28	5	2	A2+	4	-1	A2-	731095.0	[8]	1.18
2	1	E-	2	0	E+	428857.38	[15]	0.22	5	-2	B2-	4	1	B2+	733185.6	[8]	0.33
3	1	E+	3	0	E-	428892.98	[15]	0.03	5	2	B2+	4	-1	B2-	703712.5	[8]	0.74
4	1	E-	4	0	E+	428940.45	[15]	-0.20	6	-2	A2+	5	1	A2-	745652.1	[8]	1.26
5	1	E+	5	0	E-	428999.90	[15]	-0.35	6	2	A2-	5	-1	A2+	715212.8	[8]	4.63
6	1	E-	6	0	E+	429071.26	[15]	-0.49	6	-2	B2+	5	1	B2-	718448.9	[8]	2.10
7	1	E+	7	0	E-	429154.64	[15]	-0.50	6	2	B2-	5	-1	B2+	742598.5	[8]	-0.55
8	1	E-	8	0	E+	429250.17	[15]	-0.23	7	-2	A2-	6	1	A2+	730972.8	[8]	1.89
9	1	E+	9	0	E-	429357.75	[15]	0.21	7	-2	B2-	6	1	B2+	758144.0	[8]	1.00
1	-1	E-	0	0	E+	441149.58	[15]	0.44	7	2	B2+	6	-1	B2-	726612.7	[8]	1.73
2	-1	E+	1	0	E-	453482.93	[15]	0.34	8	2	A2-	7	-1	A2+	737936.0	[8]	0.10
3	-1	E-	2	0	E+	465820.50	[15]	-0.01	8	-2	B2+	7	1	B2-	743526.1	[8]	1.31
4	-1	E+	3	0	E-	478162.3	WRK	0.63	8	2	B2-	7	-1	B2+	765293.9	[8]	-0.83
5	-1	E-	4	0	E+	490505.2	WRK	0.39	9	-2	B2-	8	1	B2+	783204.9	[8]	4.38
6	-1	E+	5	0	E-	502849.7	WRK	1.03	2	-2	E+	2	-1	E-	659778.9	WRK	2.89
7	-1	E-	6	0	E+	515193.4	WRK	1.45	2	2	E-	2	1	E+	660538.0	WRK	2.14
8	-1	E+	7	0	E-	527536.9	WRK	3.54	3	-2	E-	3	-1	E+	659178.7	WRK	2.43
9	-1	E-	8	0	E+	539877.5	WRK	5.93	3	2	E+	3	1	E-	660648.3	WRK	3.64
2	-2	A2+	3	1	A2-	634590.0	[8]	-2.50	4	-2	E+	4	-1	E-	658440.1	WRK	2.76
2	-2	B2+	3	1	B2-	607318.0	[8]	-1.59	4	2	E-	4	1	E+	660793.4	WRK	3.54
2	2	B2-	3	-1	B2+	633305.1	[8]	-0.55	5	-2	E-	5	-1	E+	657590.8	WRK	2.78
3	-2	B2-	4	1	B2+	622426.4	[8]	-2.41	5	2	E+	5	1	E-	660973.7	WRK	2.14
3	2	B2+	4	-1	B2-	592927.3	[8]	-1.31	6	-2	E+	6	-1	E-	656652.2	WRK	1.23
4	-2	A2+	5	1	A2-	610301.8	[8]	-2.52	6	2	E-	6	1	E+	661190.4	WRK	0.52
4	2	B2-	5	-1	B2+	607247.3	[8]	-2.36	7	-2	E-	7	-1	E+	655640.8	WRK	-2.33
2	-2	A2+	2	-1	A2-	670757.1	[8]	-0.37	7	2	E+	7	1	E-	661442.3	WRK	-2.70
2	2	A2-	2	1	A2+	644133.3	[8]	-1.52	8	-2	E+	8	-1	E-	654570.9	WRK	-6.06
2	-2	B2+	2	-1	B2-	643415.8	[8]	-1.10	8	2	E-	8	1	E+	661729.7	WRK	-7.38
2	2	B2-	2	1	B2+	671414.8	[8]	0.79	2	2	E-	1	-1	E+	684827.0	WRK	2.56
3	-2	A2-	3	-1	A2+	642859.2	[8]	-0.94	2	-2	E+	1	1	E-	685087.1	WRK	2.80
3	2	A2+	3	1	A2-	671519.8	[8]	0.85	3	2	E+	2	-1	E-	696708.0	WRK	3.34
3	-2	B2-	3	-1	B2+	670232.4	[8]	0.62	3	-2	E-	2	1	E+	697466.8	WRK	2.61
3	2	B2+	3	1	B2-	644253.0	[8]	-1.39	9	2	E+	8	-1	E-	765241.9	WRK	-7.44
4	-2	A2+	4	-1	A2-	669565.3	[8]	0.59	9	-2	E-	8	1	E+	772371.5	WRK	-9.51
4	2	A2-	4	1	A2+	644412.4	[8]	-1.32	3	2	E-	2	2	E+	36863.510	[1]	-0.22
4	-2	B2+	4	-1	B2-	642167.6	[8]	-1.06	3	-2	E+	2	-2	E-	36863.510	[1]	-0.04
4	2	B2-	4	1	B2+	671659.4	[8]	0.62	4	2	E+	3	2	E-	49146.130	[1]	-0.12
5	-2	A2-	5	-1	A2+	641367.0	[8]	-1.43	4	-2	E-	3	-2	E+	49146.130	[1]	0.32
5	2	A2+	5	1	A2-	671832.6	[8]	-0.83	3	2	E+	2	2	E-	36928.570	[1]	-0.03
5	-2	B2-	5	-1	B2+	668777.2	[8]	1.05	3	-2	E-	2	-2	E+	36928.570	[1]	0.18
5	2	B2+	5	1	B2-	644611.4	[8]	-1.33	4	2	E-	3	2	E+	49232.470	[1]	-0.28
6	-2	A2+	6	-1	A2-	667883.5	[8]	-0.62	4	-2	E+	3	-2	E-	49232.470	[1]	0.24
6	-2	B2+	6	-1	B2-	640478.9	[8]	-1.90	3	2	E-	3	-2	E+	0.51	[1]	0.29
6	2	B2-	6	1	B2+	672042.4	[8]	-0.42	4	2	E+	4	-2	E-	0.98	[1]	0.32
7	-2	A2-	7	-1	A2+	639522.6	[8]	0.25	5	2	E-	5	-2	E+	1.76	[1]	0.21
7	-2	B2-	7	-1	B2+	666904.4	[8]	0.49	6	2	E+	6	-2	E-	2.88	[1]	-0.21
8	-2	B2+	8	-1	B2-	638504.6	[8]	-0.97	7	2	E-	7	-2	E+	4.50	[1]	-1.07
2	-2	A2+	1	1	A2-	695963.1	[8]	-0.43	8	2	E+	8	-2	E-	9.64	[1]	0.36
2	2	A2-	1	-1	A2+	668437.5	[8]	1.88	3	2	E+	3	-2	E-	0.26	[1]	0.00
2	-2	B2+	1	1	B2-	668681.7	[8]	1.56	4	2	E-	4	-2	E+	0.80	[1]	0.01
2	2	B2-	1	-1	B2+	695741.2	[8]	-0.37	5	2	E+	5	-2	E-	1.88	[1]	0.04
3	-2	A2-	2	1	A2+	681070.0	[8]	0.70	6	2	E-	6	-2	E+	3.76	[1]	0.07
3	2	A2+	2	-1	A2-	707684.0	[8]	0.09	7	2	E+	7	-2	E-	6.72	[1]	0.08
3	-2	B2-	2	1	B2+	708339.2	[8]	-0.95	8	2	E-	8	-2	E+	11.20	[1]	0.14
3	2	B2+	2	-1	B2-	680351.9	[8]	0.20	9	2	E+	9	-2	E-	17.52	[1]	0.14
4	-2	A2+	3	1	A2-	720749.1	[8]	1.23	10	2	E-	10	-2	E+	26.20	[1]	0.13
4	2	A2-	3	-1	A2+	692100.3	[8]	-0.97	11	2	E+	10	-2	E-	37.71	[1]	0.07
4	-2	B2+	3	1	B2-	693494.4	[8]	-0.04									

large amplitude motion. Instead, we chose to carry out predictions starting from the results in Ref. (*14*).

For the high J transitions, the signals in an expansion with Ar and in one with N_2 were equally strong. For the low J transitions the expansion with Ar gave much better results. This indicates that probably even higher levels than (K_a = 1, lower) can be accessed by using N_2 as a carrier gas.

The transitions were all measured with the sideband spectrometer. Predictions turned out to be correct within 400 MHz. The transitions were very weak, as expected. Signal-to-noise ratios were not better than 10 at an RC time of 3 s. The P branch could not be observed, which is consistent with Ref. (*8*) and with our measurements of the (K_a

= 0, lower) → (K_a = 1, upper) bands. The measured frequencies are listed in Table I. The combination differences with microwave transitions fitted within the experimental accuracy (1.0 MHz).

To determine the sign of the K-type doubling (which behaved unexpectedly in K_a = 1), we measured the four $Q(8)E^{\pm}$ and $R(8)E^{\pm}$ transitions. The K-type doubling in K_a = 2 is very small, but increases with $(J-1)J(J+1)(J+2)$ from 11.20 MHz for J = 8 to 17.52 MHz for J = 9 (*1*). Considering the value of the uncertainty of the measured frequencies (1.0 MHz), reliable information can be extracted from these transitions. The combination difference that can be made is

$$R(8)E^- - R(8)E^+ + Q(8)E^+ - Q(8)E^- = \pm\{(\text{doubling } J=8) + (\text{doubling } J=9)\}. \quad (1)$$

If the sign of the K-type doublings is different in (K_a = 1, lower) and (K_a = 2, upper) the sign to be used is the lower one and otherwise it is the upper one. Substitution gives in the left and right side of the equation +29.2 and +28.72 MHz, respectively. Therefore the two levels have the same K-type doubling sign.

4 ANALYSIS

For this analysis the theoretical formalism developed by Hougen (*12*) and Coudert and Hougen (*13*) was used and the same computer program as the one with which the analysis was performed in Ref. (*14*) was utilized. Details concerning the calculation of the Hamiltonian matrix elements, the size of the submatrices involved, and the way they were truncated in this computer program can be found in this reference. We were led to introduce second-order distortion terms in the asymmetric rotor Hamiltonian given in Eq. (20) of Ref. (*14*). The Hamiltonian considered for the present analysis is

$$\begin{aligned} H_{I^r} = {} & AJ_z^2 + BJ_y^2 + CJ_x^2 - D_J\mathbf{J}^4 - D_{JK}\mathbf{J}^2J_z^2 - D_KJ_z^4 + d_1\mathbf{J}^2(J_+^2 + J_-^2) \\ & + d_2(J_+^4 + J_-^4) + H_J\mathbf{J}^6 + H_{JK}\mathbf{J}^4J_z^2 + H_{KJ}\mathbf{J}^2J_z^4 + H_KJ_z^6 \\ & + f_1\mathbf{J}^4(J_+^2 + J_-^2) + f_2\mathbf{J}^2(J_+^4 + J_-^4) + f_3(J_+^6 + J_-^6), \quad (2) \end{aligned}$$

where $\mathbf{J}$, J_x, J_y, and J_z are the total angular momentum and its components and $J_\pm = J_x \pm iJ_y$. The Hamiltonian of Eq. (2) is written with Watson's S set of centrifugal parameters.

Two sets of data were included in the analysis. The first set consists of the measurements carried out in Refs. (*1*)–(*8*); the second set corresponds to the measurements reported in Ref. (*15*) along with the new frequencies presented in this paper. It is important to point out that in the first global analysis carried out by Coudert and Hougen (*14*), only the first set of data was considered. In agreement with the aforementioned authors we chose the following weights in the least-squares procedure: 2500 for the microwave data of Refs. (*1–5*); 100 for the radiofrequency data of Ref. (*1*), for the microwave data of Fraser and co-workers (*6, 7*), and for the submillimeter data reported in Ref. (*15*); and 1 for the far infrared data of Busarow *et al.* (*8*) and for the new frequencies presented in this work. The two K_a = 3 transitions of Ref. (*1*) were excluded from the fit because they gave too large an observed-minus-calculated

difference. Table I lists the assignment, the observed frequency, and the observed-minus-calculated difference for each transition. The notation used for the rotational levels is defined in Ref. (*14*). Transitions appearing both in Table I of this work and in Table II of Ref. (*14*) are assigned in the same way. However, as pointed out in this last reference, for some of these transitions the assignment is not the same as that given originally. This is true for the J assignment of one set of $\Delta J = 0$, $K_a = 2$ radiofrequency transitions of Dyke *et al.* (*1*), for the $K_a = 1$ transitions involving nondegenerate levels of Coudert *et al.* (*3*), and for the $K_a = 1$ transitions involving doubly degenerate levels of Ref. (*4, 6*) (see previous section).

Table II gives the values for the constants determined from the analysis. All the parameters mentioned in Section 2B and 2C of Ref. (*14*) as well as those from the rigid rotator of Eq. (2) were considered in preliminary fits of the data. However, only the parameters appearing in Table II were chosen in the last fitting iteration and were given nonzero value. In this table, parameters written under the "$n = 1$" label are

TABLE II

Molecular Parameters[a] for the Water Dimer

	$n = 1$[b]		$n = 4$[b]		$n = 5$[b]	
A	227 580.432 (500)	h_{4v}	-70 128.436 (104)	h_{5v}	-5 260.710 1 (177)
$\bar{B}$	6 163.846 (477)	φ_4	210.397 293° (64)	h_{5k}	32.135 (664)
B-C	26.665 (958)	θ_4	0.719 67° (365)	h_{5j}	1.268 33 (800)
D_{JK}	5.954 (917)	h_{4j}	-2.934 (254)	f_5	-0.033 08 (578)
D_J	0.048 329 (185)	f_4	-6.851 (259)	h_{5kk}	558.978 (668)
$d_1 \times 10^3$	0.345 (112)	h_{4jk}	-0.772 5 (386)	h_{5jk}	-0.462 0 (134)
$d_2 \times 10^3$	0.957 2 (112)	$\varphi_{4j} \times 10^3$	-0.984 8° (100)	$h_{5jj} \times 10^3$	-0.163 7 (308)
H_{KJ}	0.699 (200)	$\theta_{4j} \times 10^3$	-0.046 07° (233)		
$H_{JK} \times 10^3$	-0.346 (109)				
	$n = 2$[b]				$n = 7$[b]
h_{2v}	-697.583 (126)			h_{7v}	-378.000 4 (168)
θ_2	2.507 9° (574)			φ_7	126.949 72° (680)
h_{2k}	-30.280 (201)			θ_7	1.180 5° (202)
h_{2j}	-0.177 8 (184)			h_{7k}	-1 849.64 (180)
f_2	0.044 24 (934)			h_{7j}	0.143 57 (775)
h_{2jk}	0.039 07 (442)			h_{7jk}	0.273 6 (217)
$h_{2jj} \times 10^3$	-0.520 6 (714)			$\varphi_{7j} \times 10^3$	2.823 2° (549)

[a] Obtained from analysis of the transitions reported in Table I. All parameters are in MHz, except θ_2, φ_4, θ_4, θ_{4j}, φ_7 and φ_7, which are in degrees. Numbers in parentheses are one standard deviation in the same unit as the last digit.

[b] n indicated the tunneling motion $1 \rightarrow n$ to which the parameters correspond.

nontunneling usual asymmetric constants. In addition to the usual constants A, B, and C there are four first-order and two second-order distortion constants. These latter constants, H_{KJ} and H_{JK}, were not used in the analysis of Ref. (*14*). In Table II, tunneling parameters are grouped according to the tunneling motion they correspond to. These motions as well as the parameters are labeled using the numbers 2, 4, 5, or 7, the meaning of which is given in the beginning of Section 3. There are two types of tunneling parameters in Table II. The first type involves those written with Greek letters: θ_2, φ_4, φ_{4j}, θ_4, θ_{4j}, φ_7, φ_{7j}, and θ_7, which are angle-like constants necessary to account for the rotational dependence of the corresponding tunneling splitting (φ_{7j} is defined just like φ_{4j} (*14*)). A more detailed discussion of these parameters can be found in Refs. (*13, 14*). The second type of parameters involves those written with roman letters: h_{nv} is the magnitude of the tunneling splitting; h_{nk}, h_{nj}, and f_n are first-order distortion constants corresponding to the operators J_z^2, $\mathbf{J}^2$, and $(J_+^2 + J_-^2)$, respectively, in the tunneling matrix elements; and h_{nkk}, h_{njk}, and h_{njj} are second-order distortion terms corresponding to the operators J_z^4, $\mathbf{J}^2 J_z^2$, and $\mathbf{J}^4$, respectively.

Comparing Table II of the present paper and Table III of Ref. (*14*) one can see that parameters giving rise to a contribution in $J(J+1)$ to Hamiltonian matrix elements, $\bar{B}$, h_{2j}, h_{4j}, and h_{5j}, are equally well defined in both analyses. However, larger changes can be seen for the uncertainty of parameters involved in the value of the subband centers. For instance the A rotational constant and the magnitude of the $1 \rightarrow 4$ tunneling splitting, h_{4v}, have respectively an uncertainty of 0.50 and 0.10 MHz in this work and 450 and 250 MHz in Ref. (*14*). This decrease is a consequence of the fact that three additional $\Delta K_a = 1$ subbands were considered in the present analysis. The root mean square deviation of the fit for the 47 transitions weighed 2500, for the 102 transitions weighed 100, and for the 90 transitions weighed 1 is 0.080, 0.439, and 2.666 MHz, respectively.

5 DISCUSSION

The far infrared region is a rather new frequency region for high-resolution spectroscopy of van der Waals molecules. Using harmonic generation and submillimeter BWOs (both below 1000 GHz), FIR laser sidebands (below 2500 GHz) (*16*), or CO_2 laser difference frequency generation (below 6000 GHz) (*18*), very sensitive measurements can be made. However, most high-resolution spectroscopic investigations of dimers were conducted at frequencies of 1000 GHz or lower.

Van der Waals vibrations of $(H_2O)_2$ are expected in the yet unexplored regions higher than 1000 GHz. Detection of these would provide valuable information for the determination of the intermolecular potential energy surface. Further information on $K_a \geq 3$ levels in the ground vibrational state would be interesting, since the position of these cannot be predicted with high precision by existing theory, as stated above. However, the detection of transitions originating in $K_a = 2$ or higher will be difficult with the production method of dimers used in this work, since the temperature in a jet is so low that these levels are barely populated. Perhaps low temperature cells are better suited in this case.

The formalism used to analyze the data allowed us to reproduce the frequency of the observed transitions in a fairly satisfactory manner. It was possible to determine

fairly accurately and with a much smaller uncertainty than in Ref. (*14*) two important spectroscopic parameters, the A rotational constant and the magnitude of the $1 \rightarrow 4$ tunneling splitting. Also, a good understanding of the rotational dependence of the $1 \rightarrow 4$ tunneling splitting was achieved. According to Table II of Ref. (*13*), the predicted value for φ_4 is 221.907° which is in fairly good agreement with the one obtained in this analysis: 210.397°. However, several problems still remain. The first one lies in the too large number of parameters, 38, necessary to account for the frequency of the 239 transitions. The second one lies in the value of some of the distortion parameters involved in the tunneling matrix elements (h_{nk}, h_{nj}, etc.). For instance, Table II shows that the first-order distortion parameter h_{7k}, corresponding approximately to a $(K_a)^2$ contribution in the tunneling matrix element, has a value which cannot be considered as small when compared to the magnitude of the corresponding tunneling splitting, h_{7v}. These two drawbacks of the present analysis seem to indicate that, in addition to complicated tunneling–rotation Coriolis couplings for which the theoretical formalism (*13, 14*) accounts, some unusual centrifugal effects take place in the water dimer.

ACKNOWLEDGMENT

The authors are grateful to Dr. J. Hougen who had an important part in this manuscript. Further the authors thank Professor J. Reuss for his encouraging interest and E. v. Leeuwen for his technical assistance.

RECEIVED: November 13, 1990

REFERENCES

1. T. R. DYKE, K. M. MACK, AND J. S. MUENTER, *J. Chem. Phys.* **66,** 498–510 (1977).
2. J. A. ODUTOLA, T. A. HU, D. PRINSLOW, S. E. O'DELL, AND T. R. DYKE, *J. Chem. Phys.* **88,** 5352–5361 (1988).
3. L. H. COUDERT, F. J. LOVAS, R. D. SUENRAM, AND J. T. HOUGEN, *J. Chem. Phys.* **87,** 6290–6299 (1987).
4. T. A. HU AND T. R. DYKE, *J. Chem. Phys.* **91,** 7348–7354 (1989).
5. L. MARTINACHE, S. JANS-BÜRLI, B. VOGELSANGER, W. KRESA, AND A. BAUDER, *Chem. Phys. Lett.* **149,** 424–428 (1988).
6. G. T. FRASER, R. D. SUENRAM, AND L. H. COUDERT, *J. Chem. Phys.* **90,** 6077–6085 (1989).
7. G. T. FRASER, R. D. SUENRAM, L. H. COUDERT, AND R. S. FRYE, *J. Mol. Spectrosc.* **137,** 244–247 (1989).
8. K. L. BUSAROW, R. C. COHEN, G. A. BLAKE, K. B. LAUGHLIN, Y. T. LEE, AND R. J. SAYKALLY, *J. Chem. Phys.* **90,** 3937–3943 (1989).
9. Z. S. HUANG AND R. E. MILLER, *J. Chem. Phys.* **88,** 8008–8009 (1988).
10. Z. S. HUANG AND R. E. MILLER, *J. Chem. Phys.* **91,** 6613–6631 (1989).
11. T. R. DYKE, *J. Chem. Phys.* **66,** 492–497 (1977).
12. J. T. HOUGEN, *J. Mol. Spectrosc.* **114,** 395–426 (1985).
13. L. H. COUDERT AND J. T. HOUGEN, *J. Mol. Spectrosc.* **130,** 86–119 (1988).
14. L. H. COUDERT AND J. T. HOUGEN, *J. Mol. Spectrosc.* **139,** 259–277 (1990).
15. E. ZWART, J. J. TER MEULEN, AND W. L. MEERTS, *Chem. Phys. Lett.* **166,** 500–502 (1990).
16. P. VERHOEVE, E. ZWART, M. VERSLUIS, M. DRABBELS, J. J. TER MEULEN, W. L. MEERTS, A. DYMANUS, AND D. B. MCLAY, *Rev. Sci. Instrum.* **61,** 1612–1625 (1990).
17. K. L. BUSAROW, G. A. BLAKE, K. B. LAUGHLIN, R. C. COHEN, Y. T. LEE, AND R. J. SAYKALLY, *J. Chem. Phys.* **89,** 1268–1276 (1988).
18. K. M. EVENSON, D. A. JENNINGS, AND F. R. PETERSON, *Appl. Phys. Lett.* **44,** 576–578 (1984).